Next Up Previous

Next: 1 Introduction

Three-Dimensional Photolithography Simulation

Heinrich Kirchauer and Siegfried Selberherr
Institute for Microelectronics, TU Vienna, Gußhausstraße 27-29, A-1040 Vienna, Austria
Phone: +43/1/58801-3750, FAX: +43/1/5059224
E-mail: kirchauer@iue.tuwien.ac.at, WWW: http://www.iue.tuwien.ac.at

Abstract. - An overall three-dimensional photolithography simulator is presented, which has been developed for workstation based application. The simulator consists of three modules according to the fundamental processes of photolithography, namely imaging, exposure/bleaching and development. General illumination forms are taken into account. The nonlinear bleaching reaction of the photoresist is considered and electromagnetic light-scattering due to a nonplanar topography is treated by solving repeatedly the Maxwell equations within an inhomogeneous medium. A novel extension of the two-dimensional differential method into the third dimension is presented and a numerically efficient implementation for exposure simulation under partial coherent illumination is described. The development process is simulated with a cellular based surface advancement algorithm.

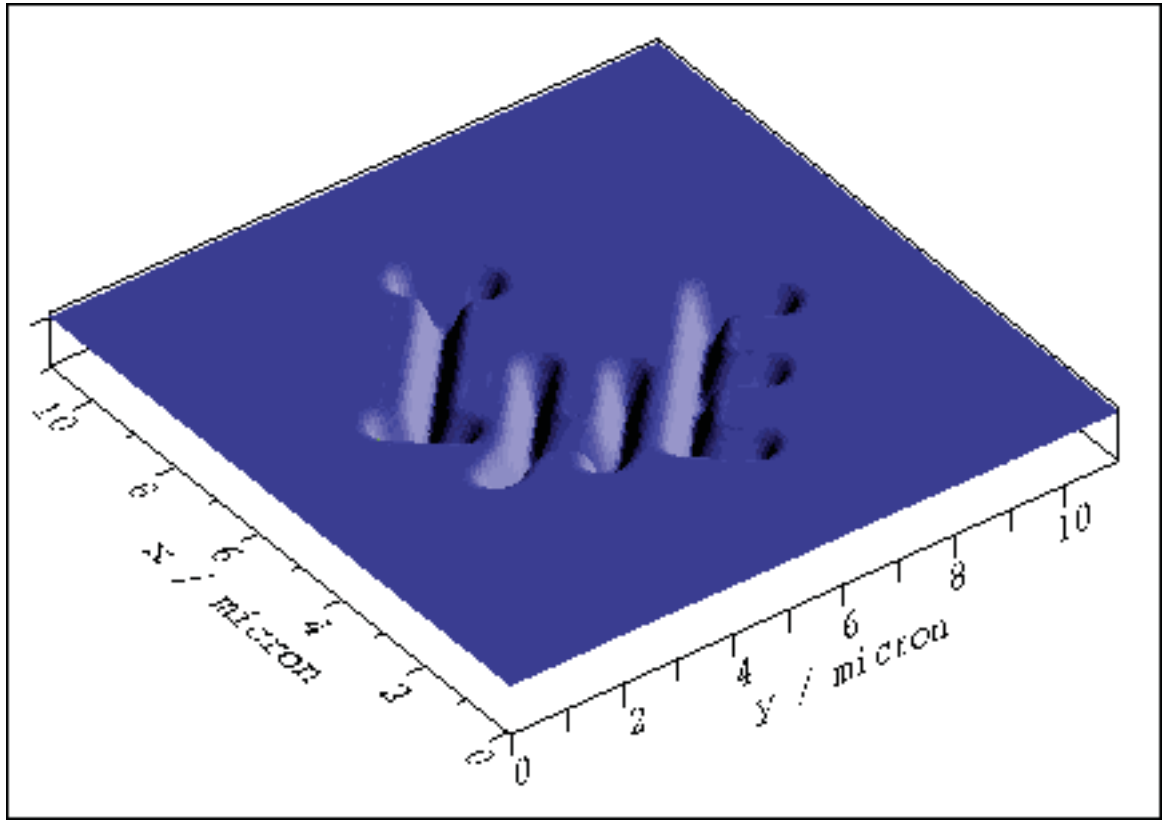

Figure 1: Aerial image of a photomask carrying the pattern $I\mu E$.

- 1 Introduction
- 2 Imaging Simulation
- 3 Exposure/Bleaching Simulation
  - 3.1 Simulation Model
  - 3.2 Numerical Solution of the Maxwell Equations
- 4 Development Simulation
- 5 Simulation of Contact Hole Printing
- 6 Conclusion
- Acknowledgement

- References

1 Introduction

Among all technologies photolithography holds the leading position in pattern transfer in today's semiconductor industry. The reduction of the lithographic feature sizes towards or even beyond the used wavelength and the increasing nonplanarity of the devices place considerable demands onto the lithography process. The large cost and time necessary for experiments make simulation an important and especially cost-effective tool for further improvements. However, a rigorous description of the fundamental physical effects governing sub-micrometer-photolithography places considerable demands onto the modeling, whereby a three-dimensional simulation becomes necessary. As a consequence the needed computational resources are extremely high. In three dimensions some approaches (e.g. [1] [2] [3]) are suited only for supercomputers, others are already proposed for workstation based simulation (e.g. [4] [5] [6]).

We present an overall three-dimensional photolithography simulator running on modern engineering workstations. The simulator consist of three different modules as shown in Fig. 2, whereby each module accounts for one of the fundamental processes of photolithography: imaging, exposure/bleaching and development.

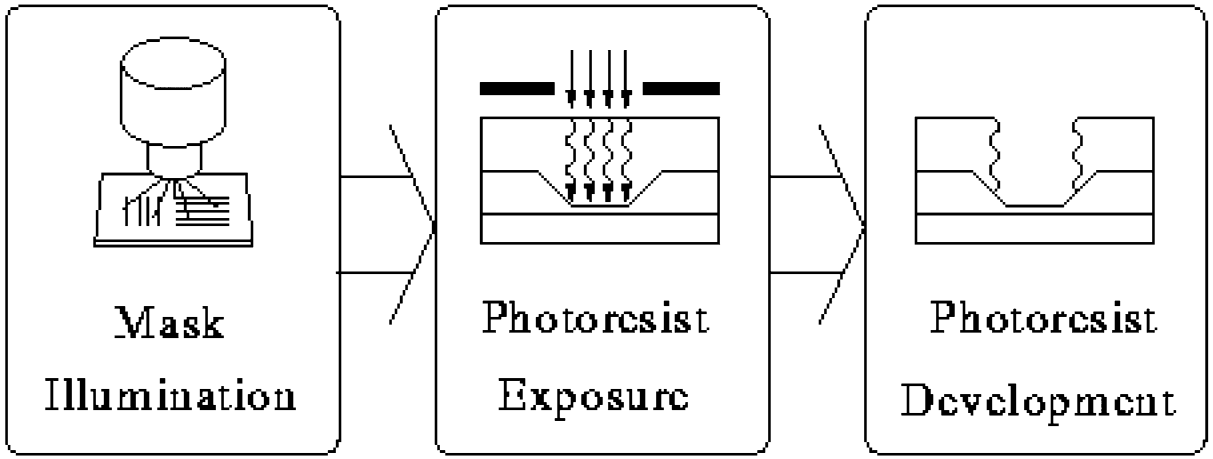

Figure 2: The three basic modules of the photolithography simulator.

The lithography simulator calls these three modules sequentially. As well defined interfaces exist between these modules, they can be treated independently. Furthermore, each part requires its specific simulation approach. The individual tasks and our solutions therefore are briefly summarized as follows:

- The imaging module describes the illumination of the photomask. The light transmission through the optical system including the photomask has to be simulated. The output of the imaging module is the aerial image, which is the light intensity incidenting on top of the wafer. Our approach combines the vector valued version [7] [8] of the classical scalar theory of Fourier optics [9] with a semi-analytical algorithm for calculating the photomask's Fourier coefficients. The discretization of the distributed light source is described in larger detail as it is of crucial importance for the numerically efficient implementation of the differential method.
- The exposure/bleaching module simulates the chemical reaction of the photosensitive resist. Thereby the light propagation within the optically nonlinear resist and electromagnetic (EM) scattering effects due a nonplanar topography have to be modeled. The result of the exposure/bleaching module is the latent bulk image. Our approach is based on the novel three-dimensional extension of the originally two-dimensional differential method. An overview of the principial operation of the algorithm is presented disregarding mathematical details but focussing on a consistent description with the imaging module.
- The development module models an isotropic etching process, whereby the inhomogeneous etch or development rate is determined by the previously calculated bulk image. The final developed resist profile is the result of the overall photolithography simulator. We extended the recently proposed cellular based etching simulator [10] [11] for photolithographic applications.

The paper is organized according to the simulation flow depicted in Fig. 2. In the next three sections we discuss the imaging, the exposure/bleaching and the development module, respectively. Then we present simulation results for contact hole printing over a planar and a stepped substrate to demonstrate the capability of the simulator. We conclude with a brief summary of the main features of the simulator and the contributions of this paper.

---

2 Imaging Simulation

In this section we describe our aerial image simulator. Although the basic concept follows the vector-valued extension [7] [8] of the scalar theory of Fourier optics [9], the module is described in greater length for the following two reasons. Firstly, the disrectization procedure of the distributed light source is of crucial importance for a numerically efficient implementation of the differential method. Secondly, a semi-analytical algorithm for the computation of the Fourier coefficients of the mask transmission function is proposed, which has the great advantage of avoiding aliasing errors due to a sampling of the mask transmission function.

To apply the concept of Fourier optics we first reduce the projection printing system to its essential parts as shown in Fig. 3.

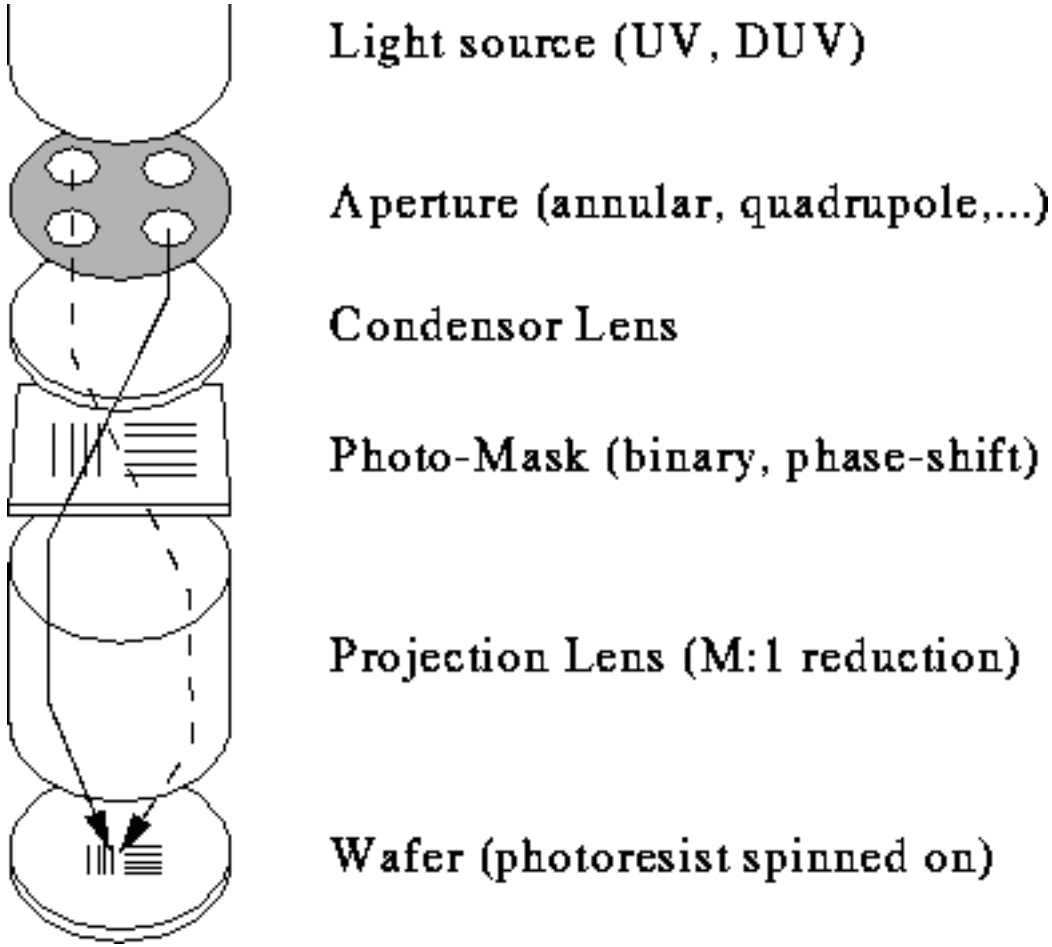

Figure 3: The projection printing system is reduced to its essential parts.

The mask-pattern is thereby assumed to be laterally periodic with periods a and b. The photomask is infinitesimally thin with ideal transitions of the transmission characteristic. The piecewise constant transmission function is real-valued (zero or one) for binary masks , in case of phase-shift masks it is complex-valued with module less or equal than one.

For the simulation of arbitrary illumination forms the distributed light source is discretized into mutually independent coherent point sources Q_{pq} . In Fig. 4 we show the discretization for an annular and a quadrupole aperture.

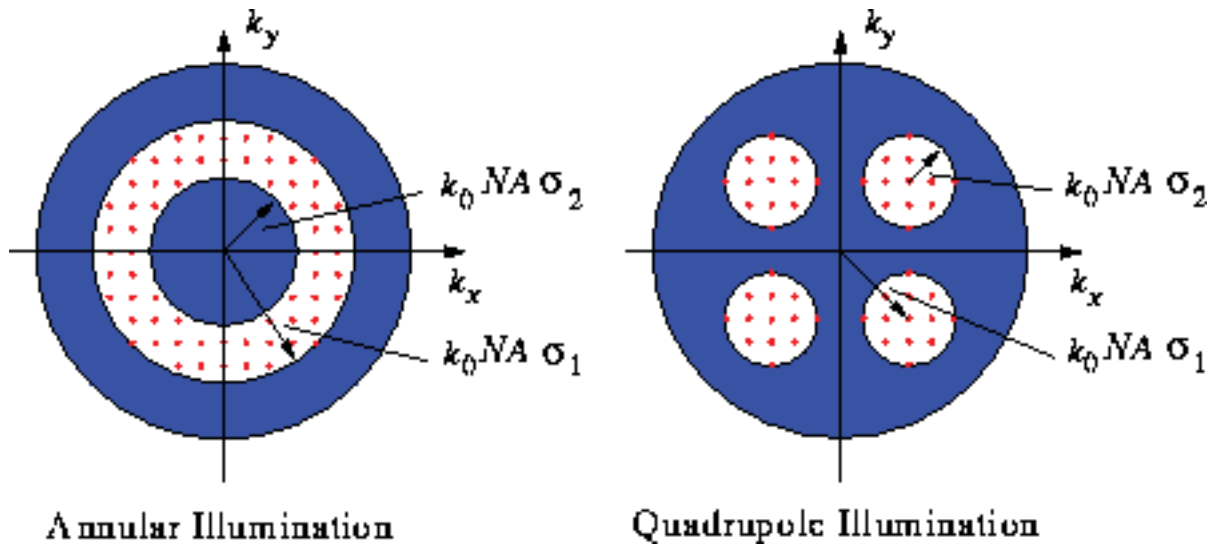

Figure 4: To account for arbitrary illumination forms the light source is discretized into mutually independent coherent point sources located inside the illumination aperture.

We choose the point source locations in such a way that all the individual contributions to the EM field are periodic. The reason therefore lies in the usage of the differential method for the exposure/bleaching module. The periodicity guarantees that the ordinary differential equation system of (6) and the boundary matrices (10) are equal for all point sources. As a consequence the linear system (12) has to be assembled just once. The additional costs due to the partial coherence lie therefore only in the solution of (12) for multiple right hand sides. Hence, the periodic requirement is essential for a numerically efficient exposure/bleaching simulation.

The spacing between the point sources Q_{pq} is chosen to assure that the lateral wavevector components k_x^{pq} and k_y^{pq} of the waves incident onto the photomask equal an integer multiple of the sampling frequencies $2\pi/a$ and $2\pi/b$ in the Fourier domain. This requirement is illustrated in the wavevector diagram of Fig. 5.

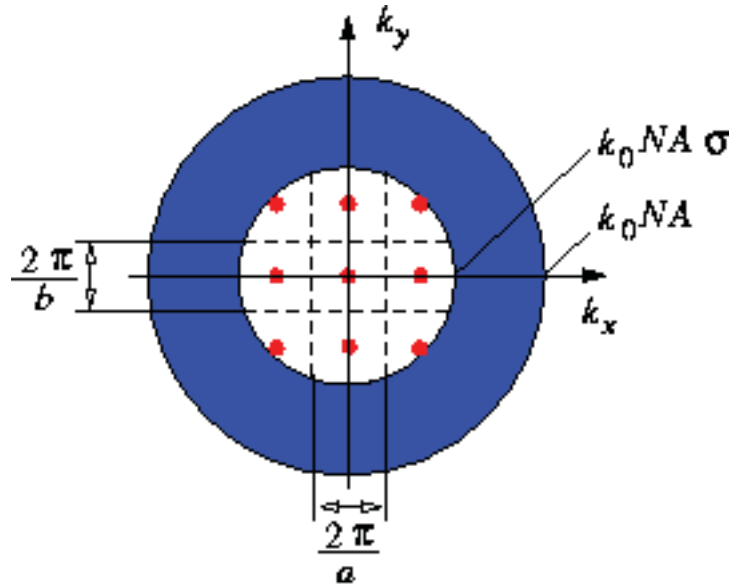

Conventional Illumination

Figure 5: The spacing between the individual point sources is chosen to yield a periodic EM field incidenting onto the photomask.

The resulting image on top of the wafer due to one coherent point source can now be expressed by a superposition of discrete diffraction orders. Because of the periodicity of the EM field this superposition corresponds to a Fourier expansion and writes to

$$\mathbf{U}^{pq}(x,y,0) = \sum_{n,m} \mathbf{U}^{pq}_{n,m}\, e^{j2\pi(n/ax+m/by)},$$

whereby $\mathbf{U}$ stands vicariously for the two EM field vectors $\mathbf{E}$ and $\mathbf{H}$. The diffraction orders are homogeneous plane waves with wavevectors $\mathbf{k}_{n,m} = 2\pi\left[n/a,\ m/b,\ \sqrt{(1/\lambda_0)^2-(n/a)^2-(m/b)^2}\right]^{\mathbf{T}}$ and amplitudes following from the vector-valued diffraction theory [7],

$$\mathbf{E}^{pq}_{nm} = T_{n-p,m-q}\,\mathbf{P}(n,m;p,q), \qquad \mathbf{H}^{pq}_{nm} = \frac{\lambda_0}{2\pi}\sqrt{\frac{\varepsilon_0}{\mu_0}}\,\mathbf{k}_{nm} \times \mathbf{E}^{pq}_{nm}. \qquad (1)$$

λ_0 is the actinic wavelength and the time dependence of the EM field is a time-harmonic one, i.e., $\mathcal{E}(\mathbf{x},t) = \mathrm{Re}\left\{\mathbf{E}(\mathbf{x})e^{-j\omega_0 t}\right\}$ and $\mathcal{H}(\mathbf{x},t) = \mathrm{Re}\left\{\mathbf{H}(\mathbf{x})e^{-j\omega_0 t}\right\}$ with angular frequency $\omega_0 = 2\pi/(\sqrt{\varepsilon_0\mu_0}\lambda_0)$.

In (1) T_{nm} stands for the Fourier coefficients of the mask transmission function. As illustrated in Fig. 6 they are computed by first triangulating the piecewise constant transmission function and then superposing weighted analytical Fourier transforms of the triangular patterns. This semi-analyitcal algorithm has the great advantage of avoiding any errors due to aliasing. Aliasing would occur by conventional sampling of the transmission function and application of the Fast Fourier Transform (FFT) algorithm, because the mask transmittance is not a low pass function [12].

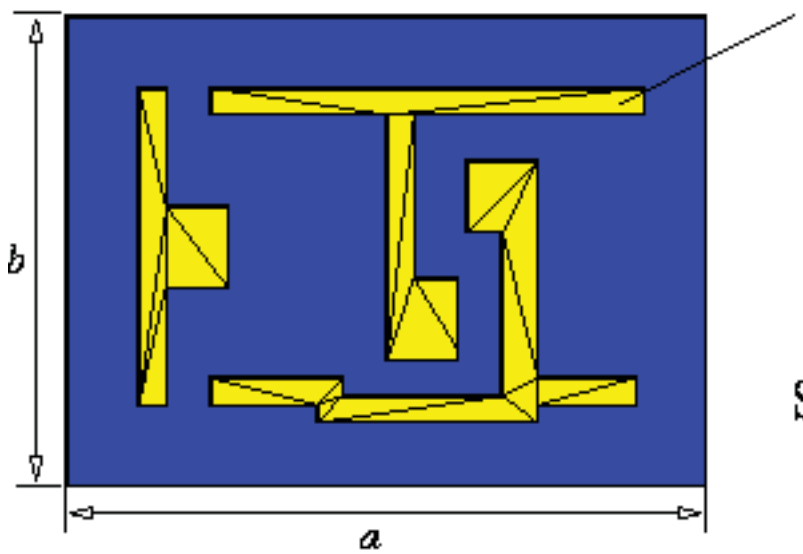

Analytical Fourier transform of k-th triangle TRI^k with transmission t_k:

$$\mathcal{T}^k_{nm} = \iint_{(x,y)\in \mathrm{TRI}^k} e^{j2\pi(nx/a+my/b)}\,dx\,dy$$

Superposition of triangle contributions $\mathcal{T}^k_{nm}$:

$$T_{nm} = \sum_k t_k\,\mathcal{T}^k_{nm}$$

Figure 6: The Fourier coefficients T_{nm} of the mask transmission function are computed analytically.

The second term $\mathbf{P}(n, m; p, q)$ of (1) is the vector-valued counterpart to the pupil-function of the scalar diffraction theory [9] and follows from ray-tracing [7] [8] trough the optical system (cf. Fig. 3). $\mathbf{P}(n, m; p, q)$ is essentially a low-pass filter (no evanescent waves can travel towards the wafer) and accounts for the polarization state, defocus and higher order aberrations terms. Hence, the vector-valued illumination spectrum (1) is band-limited and the Fourier backward transform can be accomplished using FFT techiques without any aliasing errors [12]. As the Fourier forward transform, i.e., the Fourier coefficients T_{nm} of the mask transmission function, is computed with the above described semi-analyitcal algorithm, the EM field is calculated aliasing free.

The aerial image itself is the light intensity $I(x, y)$ incidenting on top of the wafer and is thus given by the real part of the vertical component of the Poynting vector of the EM field. It is calculated by a weighted incoherent superposition of all mutually independent terms and writes to

$$I(x, y) = \sum_p \sum_q w_{pq} \mathrm{Re}\left[\mathbf{E}^{pq}(x, y, 0) \times \mathbf{H}^{pq*}(x, y, 0)\right]_z,$$

whereby the asterisk denotes complex conjugation. For a uniform bright source the weights w_{pq} are determined by the portion of the discretization rectangles $2\pi/a \times 2\pi/b$ within the illumination cone (cf. Fig. 5).

Simulation results of the aerial image module are shown in Fig. 1 and Fig. 11.

3 Exposure/Bleaching Simulation

From a simulation point of view the exposure/bleaching reaction is by far the most demanding problem within photolithography simulation. Hence, we discuss this module in greater detail. First we present the underlying physical simulation model and then come to the key point of any rigorous photolithography simulator, namely the numerical solution of the Maxwell equations.

- 3.1 Simulation Model
- 3.2 Numerical Solution of the Maxwell Equations

3.1 Simulation Model

The exposure state of the photoresist is described by the concentration of the photoactive compound (PAC) $M(\mathbf{x};t)$, which constitutes the latent bulk image. The bulk image is transferred into the photoresist by light absorption. Thereby the PAC is dissolved and the optical properties, e.g., the refractive index $n(\mathbf{x};t)$, are changed. As usually this exposure/bleaching reaction is modeled by Dill's `ABC'-model [13]

$$\frac{\partial M(\mathbf{x},t)}{\partial t} = -C\, I(\mathbf{x},t)\, M(\mathbf{x},t), \quad n(\mathbf{x},t) = n_0 + j\frac{\lambda}{4\pi}\Big(A\, M(\mathbf{x},t) + B\Big),$$

where $I(\mathbf{x},t)$ is the exposing light intensity. Consequently, the EM field inside the nonlinear photoresist has to be determined. Because the bleaching rate is small as compared to the frequency of the EM field, we apply a quasi-static approximation, i.e.,

$$M(\mathbf{x},t_{k+1}) = M(\mathbf{x},t_k)\, e^{-C\, I(\mathbf{x},t_k)\,(t_{k+1}-t_k)}, \qquad (2)$$

where the initial PAC distribution is homogeneous, $M(\mathbf{x},t_0) \equiv 1$. Furthermore, we assume a steady-state field distribution within a time step $t_k \le t < t_{k+1}$. Therefore, the EM field is time-harmonic and obeys the Maxwell equations in the form of

$$\operatorname{curl} \mathbf{H}_k(\mathbf{x}) = -j\omega_0\varepsilon_0\, \varepsilon_k(\mathbf{x})\, \mathbf{E}_k(\mathbf{x}), \qquad \operatorname{curl} \mathbf{E}_k(\mathbf{x}) = j\omega_0\mu_0\, \mathbf{H}_k(\mathbf{x}). \qquad (3)$$

THE COMPLEX PERMITTIVITY $\varepsilon_k(\mathbf{x})$ IS RELATED TO THE REFRACTIVE INDEX BY MAXWELL'S LAW, $\varepsilon_k(\mathbf{x}) = n^2(\mathbf{x}, t_k)$, AND THE EXPOSING LIGHT INTENSITY IS GIVEN BY [14]

$$I(\mathbf{x}, t_k) = \frac{1}{2}\sqrt{\frac{\varepsilon_0}{\mu_0}}\, n_0 \|\mathbf{E}_k(\mathbf{x})\|^2. \qquad (4)$$

THE EQUATION SET (2) TO (4) REPRESENTS THE SIMULATION MODEL FOR THE EXPOSURE/BLEACHING REACTION, WHEREBY AN EFFICIENT SOLUTION OF THE INHOMOGENEOUS BUT LINEAR MAXWELL EQUATIONS (3) IS THE CRUCIAL POINT FOR THE APPLICABILITY OF THE MODEL. THE PRINCIPAL SIMULATION FLOW OF THE EXPOSURE/BLEACHING MODULE IS ILLUSTRATED IN FIG. 7.

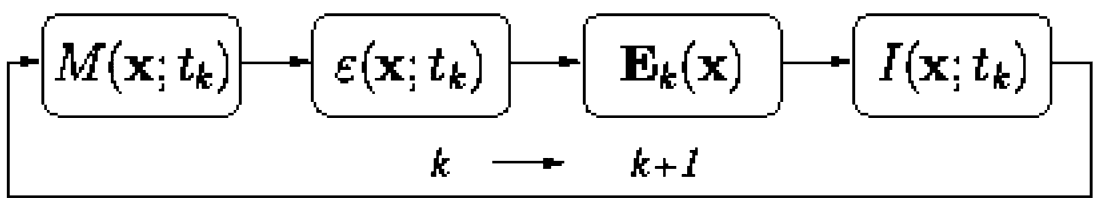

Figure 7: SIMULATION FLOW FOR THE EXPOSURE/BLEACHING MODULE.

Next Up Previous

Next: 4 Development Simulation **Up:** 3 Exposure/Bleaching Simulation **Previous:** 3.1 Simulation Model

3.2 Numerical Solution of the Maxwell Equations

Our solution of the Maxwell equations corresponds to the novel three-dimensional formulation of the differential method. This method was originally developed for the simulation of diffraction gratings [15] and was later adapted for two-dimensional photolithography simulation [7]. The differential method itself requires a rectangular shaped simulation domain ($a \times b \times h$) with periodic boundary conditions in lateral direction. Inside the simulation domain arbitrary inhomogeneous and nonplanar regions can be simulated. Above $z < 0$ and below $z > h$ multiple planar homogeneous layers form a stratified medium, that can be treated analytically and is considered by the vertical boundary conditions. A typical formation is shown in Fig. 8.

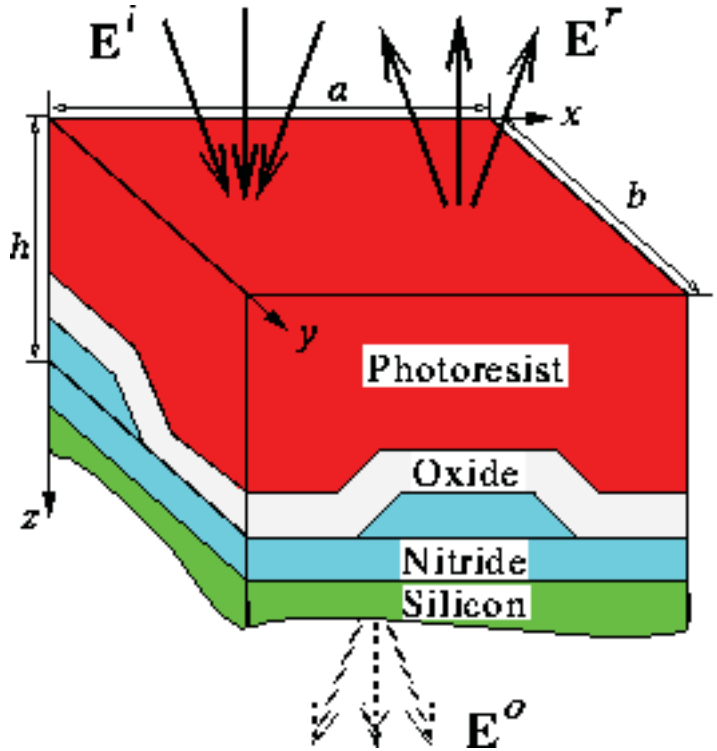

Figure 8: In the given example the simulation domain consists of the inhomogeneous photoresist, the nonplanar Oxide and the nonplanar part of the Nitride. Above $z < 0$ and below $z > h$ multiple planar homogeneous layers form a stratified medium.

The strategy behind the differential method is briefly described as follows: First, the dependency of the EM field on the lateral x- and y-coordinates is expressed by Fourier series. Insertion of these expansions into the Maxwell equations transforms the partial differential equations (PDEs) into a system of ordinary differential equations (ODEs). Once the boundary conditions (BCs) are determined and the ODE system is solved, the obtained field coefficients are transformed back to the spatial domain. A schematic overview of the various steps involved in the numerical algorithm is illustrated in Fig. 9.

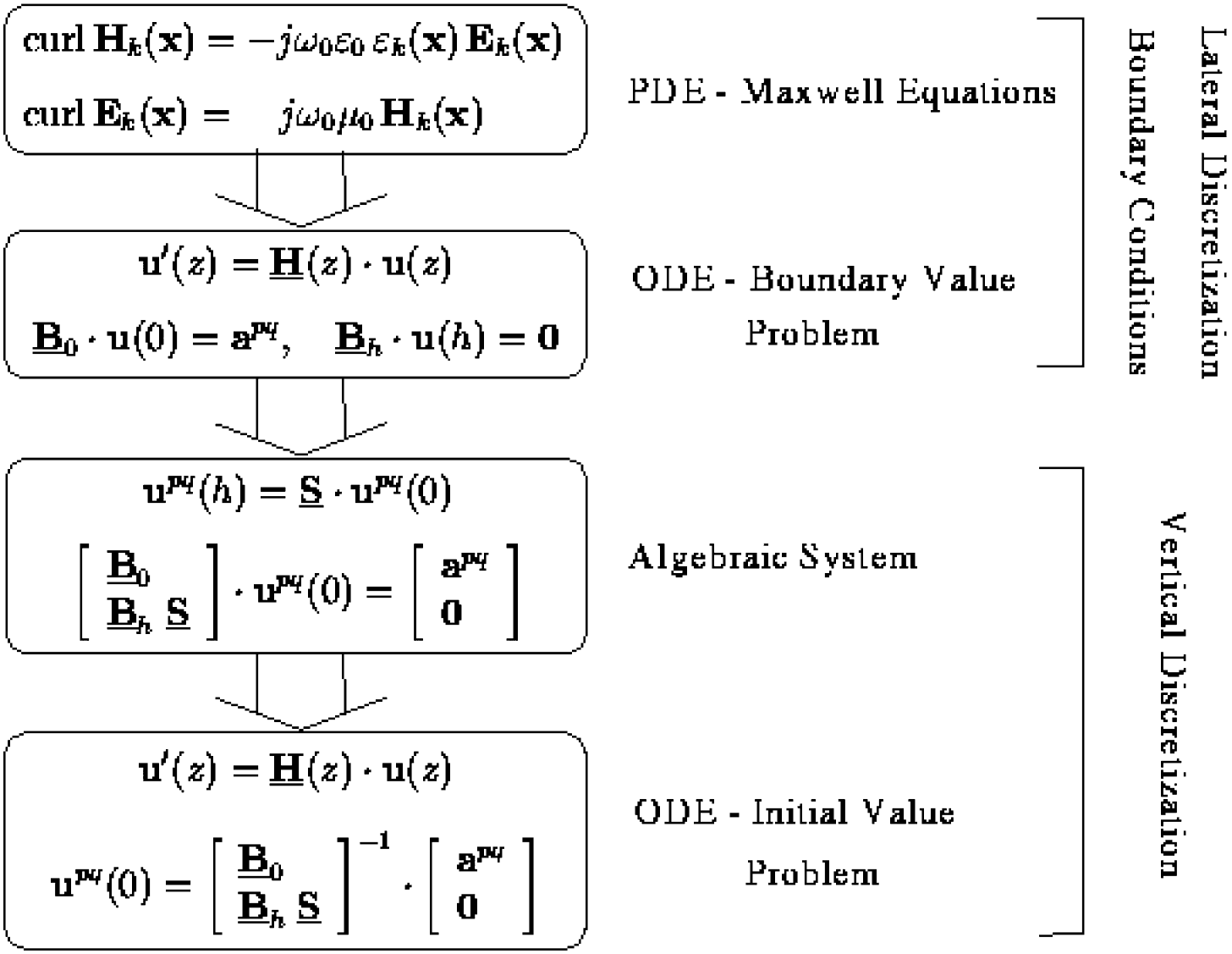

Figure 9: Overview of the numerical algorithm.

A more detailed discussion of the <u>lateral discretization</u>, the <u>boundary conditions</u>, and the <u>vertical discretization</u> is presented in the following three items:

- **Lateral Discretization:** Due to the periodic nature of the <u>incident light</u> and the assumed lateral periodicity of the <u>simulation domain</u> the EM field as well as the permittivity inside the simulation domain can be expressed by Fourier series,

$$\varepsilon(\mathbf{x}) = \sum_{n,m} \varepsilon_{nm}(z) e^{j2\pi(nx/a+my/b)}, \ \mathbf{U}(\mathbf{x}) = \sum_{n,m} \mathbf{U}_{nm}(z) e^{j2\pi(nx/a+my/b)}. \quad (5)$$

Here, it is most important to emphasize that the above expansions are valid for all point sources Q_{pq} and time steps t_k .

Insertion of (5) into (3) transforms the PDEs into an infinite dimensional set of coupled ODEs for the Fourier coefficients of the lateral field components, as the vertical field components can be expressed analytically by the lateral ones. Next, the Fourier expansions of (5) are truncated. Thus, only coefficients $\{E_{x,nm}, E_{y,nm}, H_{x,nm}, H_{y,nm}\}_{|n|\leq N_x, |m|\leq N_y}$ symmetrically centered around the vertical incident ray n=m=0 are related by the final ODE-system,

$$\frac{d}{dz}\mathbf{u}(z) = \underline{\mathbf{H}}(z) \cdot \mathbf{u}(z) \qquad \text{with} \qquad \underline{\mathbf{H}}(z) = \begin{bmatrix} \underline{\mathbf{0}} & \underline{\mathbf{R}}(z) \\ \underline{\mathbf{G}}(z) & \underline{\mathbf{0}} \end{bmatrix}. \quad (6)$$

In the above matrix-vector notation the complex-valued vector $\mathbf{u}(z) = [\mathbf{e}_x(z), \ \mathbf{e}_y(z), \ \mathbf{h}_x(z), \ \mathbf{h}_y(z)]^{\mathbf{T}}$ comprises the Fourier coefficients of the lateral field components, e.g. $(\mathbf{e}_x(z))_k = E_{x,n(k)m(k)}(z)$, and the elements $\underline{\mathbf{R}}(z)$ and $\underline{\mathbf{G}}(z)$ of the system matrix $\underline{\mathbf{H}}(z)$ contain the Fourier coefficients of the permittivity $\varepsilon(\mathbf{x})$. Each of the **e** and **h** vectors has dimension $(2N_x + 1) \times (2N_y + 1)$ due to the symmetric truncation. Therefore, the entire ODE system is of dimension

$$N_{\text{ODE}} = 4 \times (2N_x + 1) \times (2N_y + 1) \approx 16 \times N_x \times N_y. \quad (7)$$

- **Boundary Conditions:** Above and below the simulation domain we have homogeneous planar layers (cf. Fig.

8). Inside one layer the EM field can be expressed by a plane wave or Rayleigh expansion [16]. The mathematical formulation is that of a Fourier series with vertically known dependency of the coefficients. Above the simulation domain ($z < 0$) we have to consider incident and reflected waves,

$$\mathbf{U}(\mathbf{x}) = \sum_{|n| \le N_x} \sum_{|m| \le N_y} \left[\mathbf{U}^i_{nm} e^{jk^0_{z,nm} z} + \mathbf{U}^r_{nm} e^{-jk^0_{z,nm} z} \right] e^{j2\pi(nx/a + my/b)}, \qquad (8)$$

below ($z < 0$) only outgoing waves occur disregarding multiple planar layers,

$$\mathbf{U}(\mathbf{x}) = \sum_{|n| \le N_x} \sum_{|m| \le N_y} \mathbf{U}^o_{nm} e^{jk^s_{z,nm}(z-h)} e^{j2\pi(nx/a + my/b)}. \qquad (9)$$

The extension to the general situation of a vertically stratified medium is straight forward [16] and therefore skipped in this paper. Matching the two Rayleigh expansions (8) and (9) with the field representation (5), valid inside the simulation domain, and eliminating the unknown reflected and outgoing wave amplitudes, $\mathbf{U}^r_{nm}$ and $\mathbf{U}^o_{nm}$, respectively, yields exactly half of the BCs at the top (z=0) and at the bottom (z=h) of the simulation domain. The incident amplitudes $\mathbf{U}^i_{nm}$ are of course involved in the BCs as the excite the EM field inside the simulation domain. They are the output of the illumination simulation and given by (1). This means that we have different excitation vectors for each coherent point source Q_{pq} . Using the above introduced vector notation we find

$$\underline{\mathbf{B}}_0 \cdot \mathbf{u}(0) = \mathbf{a}^{pq}, \qquad \underline{\mathbf{B}}_h \cdot \mathbf{u}(h) = \mathbf{0}. \qquad (10)$$

However, the two rectangular matrices $\underline{\mathbf{B}}_0$ and $\underline{\mathbf{B}}_h$ are independent of the specific Q_{pq}, whereas the excitation vector $\mathbf{a}^{pq}$ comprises the incoming wave amplitudes $\mathbf{E}^{pq}_{nm}$ and $\mathbf{H}^{pq}_{nm}$ of one coherent point source contribution. This means, that we have transformed the Maxwell equations (3) into a linear complex-valued two-point boundary value problem (6) and (10) with multiple BCs.

- **Vertical Discretization:** We adapted the memory saving ``shooting method'' [17] as it allows a very efficient

treatment of the multiple right hand sides of the first BC in (10). The algorithm is based on the observation, that the system matrix $\underline{\mathbf{H}}(z)$ in (6) as well as the two boundary matrices $\underline{\mathbf{B}}_0$ and $\underline{\mathbf{B}}_h$ of (10) are independent of the chosen point source. This property is a direct consequence of the special source discretization procedure yielding a periodic incident field as discussed below Fig. 4.

Exploiting this situation, we first establish a relation between the two boundary points z=0 and *z*=h, which is accomplished by applying an explicit discretization scheme to (6). The obtained recursion formula $\mathbf{u}(z_{j+1}) = \underline{\mathbf{S}}_j \cdot \mathbf{u}(z_j)$ between two adjacent mesh points is then successively evaluated,

$$\mathbf{u}(h) = \left[\prod_{j=0}^{N_z-1} \underline{\mathbf{S}}_j \right] \cdot \mathbf{u}(0) = \underline{\mathbf{S}} \cdot \mathbf{u}(0), \qquad (11)$$

whereby N_z is the number of vertical discretization points. Combining this equation with the second BC of (10) yields $\underline{\mathbf{B}}_h \cdot \mathbf{u}(h) = \underline{\mathbf{B}}_h \, \underline{\mathbf{S}} \cdot \mathbf{u}(0) = \mathbf{0}$, which forms together with the first BC of (10) a linear algebraic system for the initial values $\mathbf{u}^{pq}(0)$ due to one excitation vector $\mathbf{a}^{pq}$,

$$\begin{bmatrix} \underline{\mathbf{B}}_0 \\ \underline{\mathbf{B}}_h \, \underline{\mathbf{S}} \end{bmatrix} \cdot \mathbf{u}^{pq}(0) = \begin{bmatrix} \mathbf{a}^{pq} \\ \mathbf{0} \end{bmatrix}. \qquad (12)$$

This linear system is solved by performing a LU decomposition, which is an extremely efficient solution method for linear systems with multiple right hand sides [18]. Once the initial values $\mathbf{u}^{pq}(0)$ are found, the solution vector $\mathbf{u}^{pq}(z_j)$ inside the simulation domain is calculated by integrating the ODE system (6). As the elements of $\mathbf{u}^{pq}(z_j)$ correspond to the Fourier coefficients of the EM field, they have to be transformed back to the spatial domain. Finally, the point source contributions are incoherently superposed to build up the absorbed light intensity within the photoresist, which is needed in (4) for the exposure/bleaching model.

The proposed algorithm has the great advantage that the vertical mesh size N_z does not influence the storage consumption as the recursion matrices $\underline{\mathbf{S}}_j$ in (11) do not have to be stored individually. The memory usage is therefore only determined by the rank N_{ODE} of the ODE system (7) and is of order $\mathcal{O}(N_{\mathrm{ODE}}^2) \approx 256 \times \mathcal{O}(N_x^2 \times N_y^2)$. Typically 31 Fourier coefficients are needed

for each lateral direction. In this case $N_x = N_y = 15$ and the ODE system is of rank $N_{\mathrm{ODE}} = 3844$. Assuming 16 Bytes for a double precision complex number, approximately 250 MB memory are required to store the system matrix. For three-dimensional rigorous photolithography simulation this storage consumption is in accordance with other frequency-domain methods (e.g., [6]), and lies dramatically below time-domain methods (e.g., [3]).

For the investigation of the numerical costs we have to bear in mind, that the Maxwell equations (3) have to be solved for multiple time steps (cf. Fig. 7). The numerical costs for one time step are mainly determined by the evaluation of the recursion (11) and by the solution of (12). Both operations are of order $\mathcal{O}(N_{\mathrm{ODE}}^3)$. Hence, the total run-time grows for N_t time steps and N_z vertical discretization points with $\mathcal{O}(N_t \times N_z \times N_{\mathrm{ODE}}^3)$ and is typically under a few hours on a DEC-600 workstation. Finally it is worth mentioning, that the number of simulated point sources does not significantly influence the simulation time, which is an unique feature of the proposed discretization method.

---

4 Development Simulation

The development of the photoresist is modeled as a surface-controlled etching reaction [13]. We use Kim's `R'-model to relate the bulk image to a spatially inhomogeneous etch or development rate [19]. This development rate is stored on a tensorproductgrid, because the above discussed differential method requires a laterally uniform spaced grid to apply the numerically highly efficient two-dimensional FFT algorithm. For the simulation of the time-evolution of the development front we have adapted the recently proposed cellular-based topography simulator of [10] [11] to read the development rate from the tensorproductgrid. The basic idea behind this surface advancement algorithm is to apply a structuring element along the exposed surface which removes successively photoresist cells of the underlying cellular geometry representation. Within the scope of lithography simulation the shape of the structuring element depends on the precalculated development rate multiplied by the chosen time step. The principal operation of the algorithm is illustrated in Fig. 10.

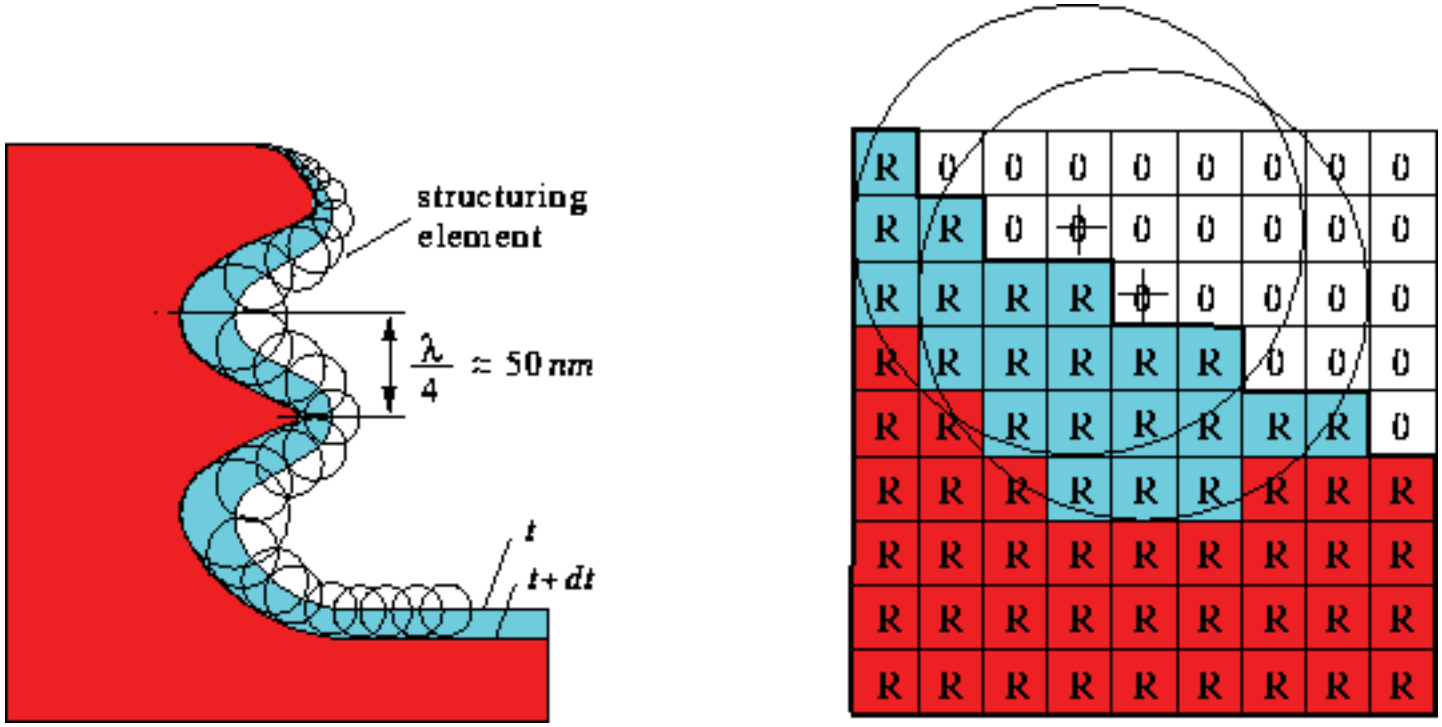

Figure 10: The structuring element walks along the exposed surface and cells within the structuring element are removed.

As the development rate exhibits a strong dependence on the spatial coordinates, e.g., due to standing waves or notching effects during photoresist exposure, a sufficiently high number of cells has to be chosen to resolve these variations. For example, in case of standing waves we know that the distance between the maxima and minima of the absorbed light intensity and therefore also of the development rate is $\lambda/4$ yielding approximately $50\,nm$ for I-line illumination ($\lambda = 365\,nm$) and a refractive index of $n_o = 1.8$ for the photoresist (c.f. Fig. 10).

For an accurate movement of the development front the structuring element must not be larger than this significant distance. In [10] and [11] it is shown, that the structuring element should be resolved with approximately 15 cells to avoid rounding and faceting errors. Hence, at least a cell density of 300 cells/μm is needed for photolithographic applications. The applicability of the structuring element algorithm for such a cellular geometry resolution has already been demonstrated in [10] and [11]. A further discussion of accuracy issues and rounding effects as well as a comparision to other surface advancement algorithms (e.g., string, ray-trace and cell-removal algorithm) can be found in [20].

H. Kirchauer and S. Selberherr: Three-Dimensional Photolithography Simulation

5 Simulation of Contact Hole Printing

To demonstrate the capability of our approach we simulated contact hole printing over a planar and a stepped topography. In both cases the simulation domain was $1.5\,\mu m \times 1.5\,\mu m \times 1.0\,\mu m$ large and the bulk material underneath was Silicon with a refrative index of $n_{Si} = 6.522 + j2.705$. In the nonplanar case the Oxide step with a refractive index of $n_{SiO2} = 1.47$ was centered in the middle of the simulation domain, the height was $0.33\mu m$ and the slope was 45°.

For the imaging and exposure/bleaching simulation 31 Fourier modes or $N_x = N_y = 15$ were used to represent the EM field consuming 250 MB memory. The number N_z of vertical discretization points was 100 and 5 time steps were used for the bleaching reaction. The run time was about 6 hours on DEC-600 workstation. The development simulation was performed with a cell density of 300 cells/μm. The memory usage was 60 MB assuming 1 Byte per cell and the run time was 30 minutes on a DEC-600 workstation.

In Fig. 11 we show the aerial image obtained with the vector-valued approach used for our imaging module. Conventional I-line illumination with a numerical aperture of NA = 0.5 and a partial coherence factor of $\sigma = 0.7$ was used. Nine mutually incoherent point sources were needed to account for the partial coherence. The point source location is shown in the wavevector diagram of Fig. 5.

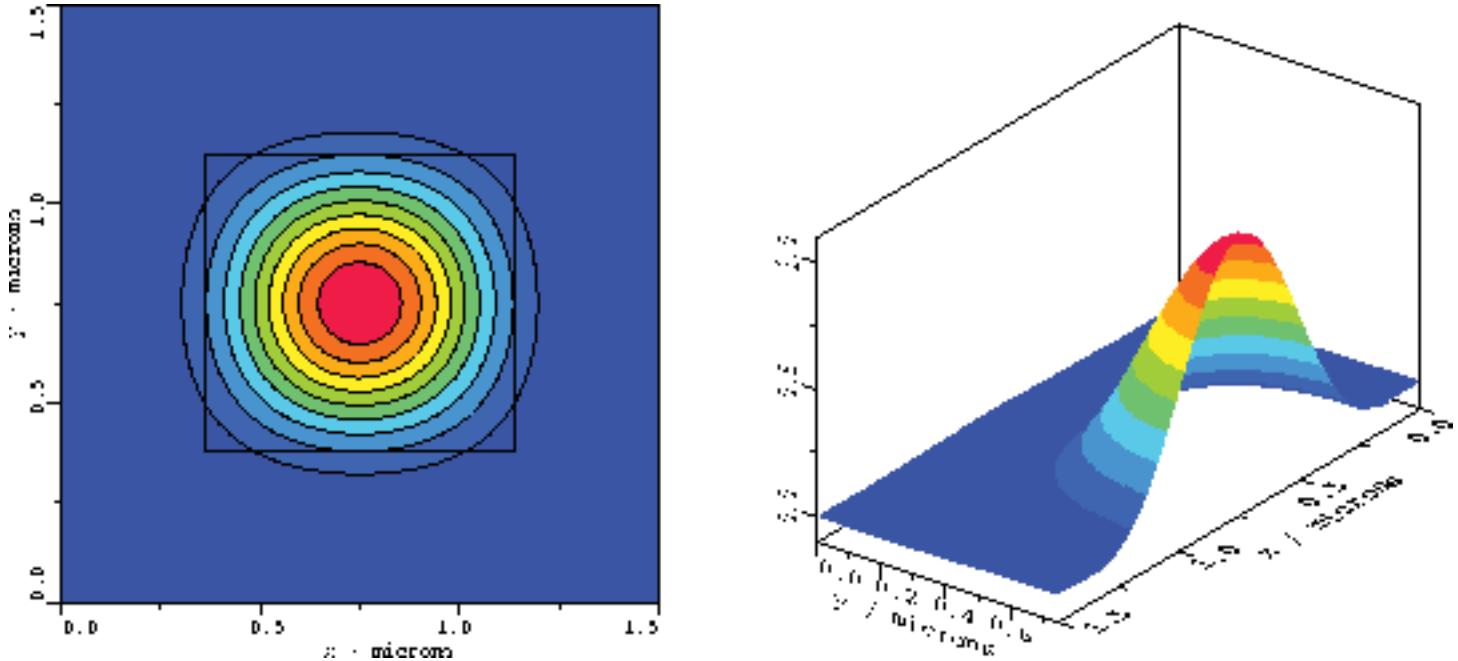

Figure 11: AERIAL IMAGE OF A $0.75\,\mu m \times 0.75\,\mu m$ WIDE CONTACT HOLE CENTERED IN THE MIDDLE OF THE $1.5\,\mu m \times 1.5\,\mu m$ LARGE SIMULATION DOMAIN.

IN FIG. 12 CONTOUR PLOTS OF THE PAC ARE SHOWN IN THE UPPER TWO FIGURES AND THE DEVELOPED PHOTORESIST PROFILES IN THE LOWER TWO FIGURES. THE CONTOURS ARE GIVEN FOR PAC = $0.2,\ 0.3,\ \ldots,\ 1.0$. THE EXPOSURE-DOSE WAS $120\,mJ/cm^2$ AND THE DEVELOPMENT TIME WAS $50\,sec$. THE SIMULATION PARAMETERS WERE FOR THE DILL-MODEL $n_0 = 1.65$, $A = 0.55\,\mu m^{-1}$, $B = 0.045\,\mu m^{-1}$, $C = 0.013\,cm^2/mJ$ AND FOR THE KIM-MODEL $R_1 = 0.25\,\mu m/sec$, $R_2 = 0.0005\,\mu m/sec$, $R_3 = 7.4$ (CF. TABLE IV IN [19]).

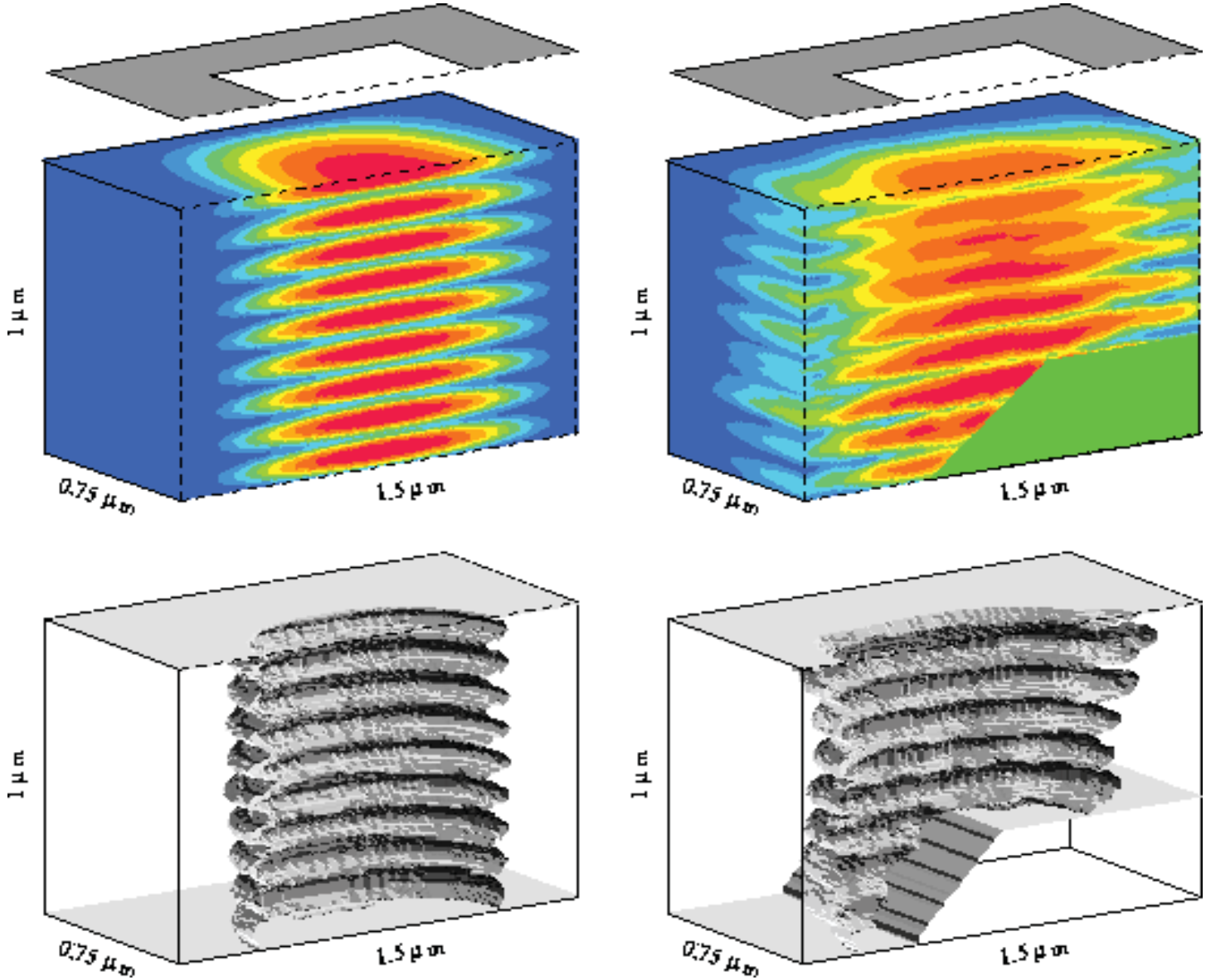

Figure 12: Bulk image and developed photoresist profile over a planar and a nonplanar substrate.

The oval contours are caused from standing waves within the photoresist, which result from substrate reflections. Due to the lateral variation in optical thickness the regular shaped bulk image and resist profile of the planar topography is distorted in case of the stepped topography. Futhermore, the opening for the stepped substrate is wider than for the planar substrate. Hence, the effective diameter of the contact hole depends on

the nonplanarity of the wafer topography.

Further comparisons with experiments are not given as the main scope of this paper is to present the overall three-dimensional lithography simulator and to demonstrate its applicability for rigorous three-dimensional workstation based simulation. The intrinsic physical correctness of the various simulation models has already been demonstrated elsewhere (e.g., for the imaging and exposure/bleaching module in [7] and for the development module in [11]) and can therefore be taken as granted.

Next Up Previous

Next: 6 Conclusion **Up:** Abstract **Previous:** 4 Development Simulation

---

6 Conclusion

An overall three-dimensional workstation based photolithography simulator has been presented, that accounts for all of the three lithography subprocesses of mask imaging, resist exposure/bleaching and resist development. The imaging simulation relies on a vector-valued reformulation of the classical scalar theory of Fourier optics. The source discretization algorithm is especially adjusted to ensure an efficient exposure simulation under partial coherent illumination. A semi-analytical method to calculate the Fourier coefficients of the mask transmission function is proposed, that avoids any aliasing errors due to sampling of the non band-limited mask transmission function. The exposure/bleaching module extends the two-dimensional differential method to the third dimension. This novel three-dimensional extension was shown to be extremely efficient for the simulation of nonplanar scattering effects in combination with partial coherent illumination. For the development/etching step a cellular based topography simulator was adapted for lithography specific requirements such as rapid varying inhomogeneous etch rates. The capability of the overall simulator was demonstrated by showing simulation results of contact hole printing over a planar and a stepped substrate.

Acknowledgment

This research project is significantly supported by Austria Mikro Systeme International AG, Unterpremstätten, Austria and Christian Doppler Forschungsgesellschaft, Vienna, Austria.

Next Up Previous

Next: 1 Introduction

Three-Dimensional Photolithography Simulation

Heinrich Kirchauer and Siegfried Selberherr
Institute for Microelectronics, TU Vienna, Gußhausstraße 27-29, A-1040 Vienna, Austria
Phone: +43/1/58801-3750, FAX: +43/1/5059224
E-mail: kirchauer@iue.tuwien.ac.at, WWW: http://www.iue.tuwien.ac.at

Abstract. - An overall three-dimensional photolithography simulator is presented, which has been developed for workstation based application. The simulator consists of three modules according to the fundamental processes of photolithography, namely imaging, exposure/bleaching and development. General illumination forms are taken into account. The nonlinear bleaching reaction of the photoresist is considered and electromagnetic light-scattering due to a nonplanar topography is treated by solving repeatedly the Maxwell equations within an inhomogeneous medium. A novel extension of the two-dimensional differential method into the third dimension is presented and a numerically efficient implementation for exposure simulation under partial coherent illumination is described. The development process is simulated with a cellular based surface advancement algorithm.

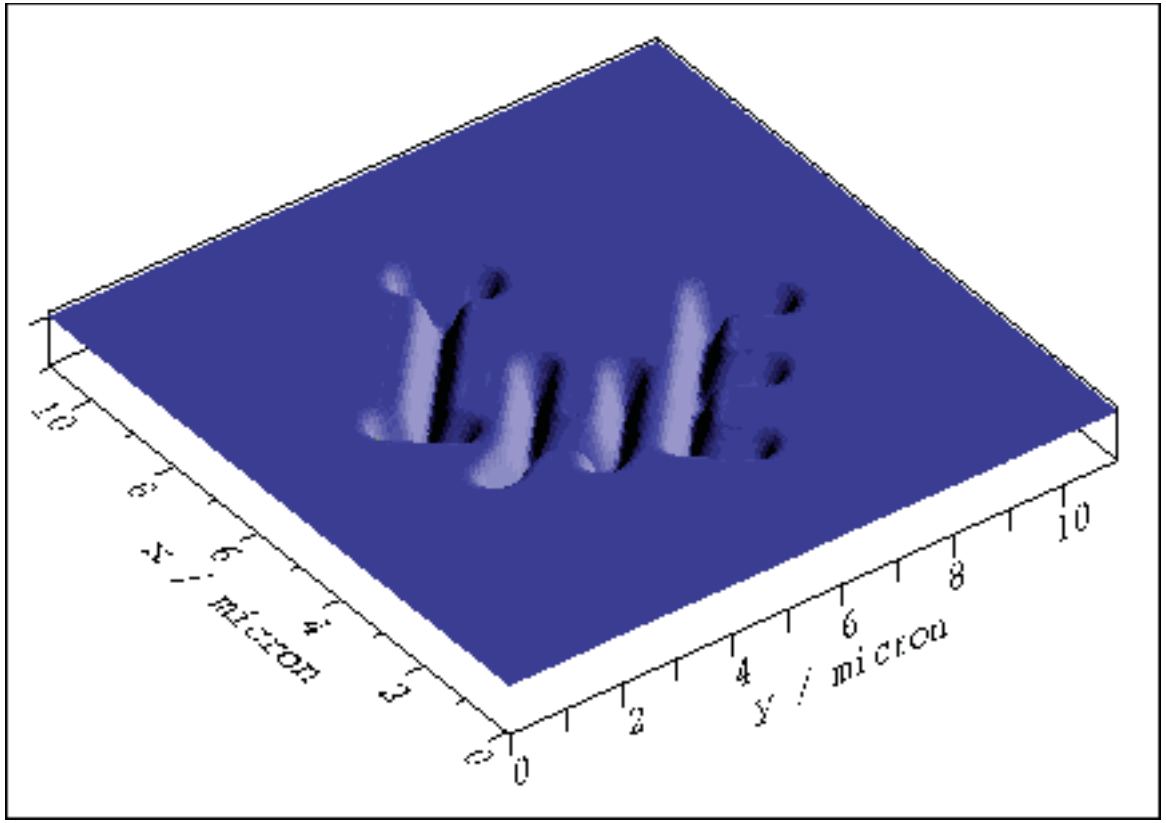

Figure 1: Aerial image of a photomask carrying the pattern $I\mu E$.

- 1 Introduction
- 2 Imaging Simulation
- 3 Exposure/Bleaching Simulation
  - 3.1 Simulation Model
  - 3.2 Numerical Solution of the Maxwell Equations
- 4 Development Simulation
- 5 Simulation of Contact Hole Printing
- 6 Conclusion
- Acknowledgement

- References

References

1

R. Guerrieri, K.H. Tadros, J. Gamelin, and A.R. Neureuther, ``Massively parallel algorithms for scattering in optical lithography'', IEEE Trans.Computer-Aided Design, vol. 10, no. 9, pp. 1091-1100, 1991.

2

A.K. Wong, R. Guerrieri, and A.R. Neureuther, ``Massively parallel electromagnetic simulation for photolithographic applications'', IEEE Trans.Computer-Aided Design, vol. 14, no. 10, pp. 1231-1240, 1995.

3

A.K. Wong and A.R. Neureuther, ``Rigorous three-dimensional time-domain finite-difference electromagnetic simulation for photolithographic applications'', IEEE Trans.Semiconductor Manufacturing, vol. 8, no. 4, pp. 419-431, 1995.

4

C.M Yuan, ``Efficient light scattering modeling for alignment, metrology, and resist exposure in photolithography'', IEEE Trans.Electron Devices, vol. 39, no. 7, pp. 1588-1598, 1992.

5

H. Tanabe, ``Modeling of optical images in resists by vector potentials'', in Proc.SPIE: Optical/Laser Microlithography V, vol. 1674, pp. 637-649, 1992.

6

K.D. Lucas, H. Tanabe, C.M. Yuan, and A.J. Strojwas, ``Efficient and rigorous 3D model for optical lithography simulation'', in Proc. Simulation of Semiconductor Devices and Processes, vol. 6, pp. 14-17, 1995.

7

M.S.C. Yeung, ``Modeling high numerical aperture optical lithography'', in Proc.SPIE: Optical/Laser Microlithography, vol. 922, pp. 149-167, 1988.

8

E. Wolf, ``Electromagnetic diffraction in optical systems I: An integral representation of the image field'', in Proc.Royal Soc.London, vol. A-253, pp. 349-357, 1959.

9

J.W. Goodman, Introduction to Fourier Optics, McGraw-Hill, N.Y., 1968.

10

E. Strasser, G. Schrom, K. Wimmer, and S. Selberherr, ``Accurate simulation of pattern transfer processes using Minkowski operations'', IEICE Transactions on Electronics, vol. E77-C, pp. 92-97, 1994.

11

E. Strasser and S. Selberherr, ``Algorithms and models for cellular based topography simulation'', IEEE Trans.Computer-Aided Design, vol. 14, no. 9, pp. 1104-1114, 1995.

12

V. Axelrad, ``Fast and accurate aerial imaging simulation for layout printability optimization'', in Proc. Simulation of Semiconductor Devices and Processes, vol. 6, pp. 10-13, 1995.

13

F.H. Dill, ``Optical lithography'', IEEE Trans.Electron Devices, vol. ED-22, no. 7, pp. 440-444, 1975.

14

D.A. Bernard, ``Simulation of focus effects in photolithography'', IEEE Trans.Semiconductor Manufacturing, vol. 1, no. 3, pp. 85-97, 1988.

15

R. Petit, Electromagnetic Theory of Gratings, Springer, 1980.

16

M. Born and E. Wolf, Principles of Optics, Pergamon Press, 6th edition, 1993.

17

U.M. Ascher, R.M.M. Mattheij, and R.D. Russel, Numerical Solution of Boundary Value Problems for Ordinary Differential Equations, Classics in Applied Mathematics. SIAM, 1995.

18

G.H. Golub and C.F. Van Loan, Matrix Computations, John Hopkins University Press, second edition, 1989.

19

D.J. Kim, W.G. Oldham, and A.R. Neureuther, ``Development of positive photoresist'', IEEE Trans.Electron Devices, vol. ED-31, no. 12, pp. 1730-1736, 1984.

20

E. Strasser, Simulation von Topographieprozessen in der Halbleiterfertigung, Chapter 3.6, PhD thesis (HTML document, in German), TU Vienna, Vienna, Austria, 1994.